Journal of the Brazilian Society of Mechanical Sciences and Engineering (2021) 43:169
https://doi.org/10.1007/s40430-021-02890-0

TECHNICAL PAPER

Numerical studies of laminar flow over two tandem elliptical cylinders using Ramanujan approximation

Javad Farrokhi Derakhshandeh[1] · **Nima Gharib**[1]

Received: 4 October 2020 / Accepted: 12 February 2021 / Published online: 27 February 2021

Abstract

This paper studies a laminar flow over tandem elliptical cylinders at Re = 200. While the aspect ratio (*AR*) of the upstream cylinder varies from $AR = a_1/b_1 = 0.25$ to 2.00, the aspect ratio of the downstream cylinder is kept constant at $AR = 1.00$ (e.g., $a_2/b_2 = 1$). This range of *AR* covers the most important practical cross sections of elliptical cylinders, including normal elliptic cylinder (with 90° incidence) and parallel elliptic cylinders (with 0° incidence). Although the spacing ratio between the centers of the cylinders is kept constant at $L^* = 4D_2$, the gap ratio ($G^* = G/D_2$) between the surfaces of the cylinders is varied due to the alteration of *AR* of the upstream cylinder. Unlike the previously published studies, which estimated the hydraulic diameter of the elliptical cylinder, in this paper, the precise hydraulic diameter is evaluated and used to analyze the wake instabilities and the variation of the imposed pressure as well as forces coefficients on the cylinders. The results reveal that with the estimation of the hydraulic diameter of the elliptic cylinder, the maximum error of 178% has arisen, which significantly affects forces (lift and drag) coefficients. It was found that the phase lag between the sinusoidal lift coefficients of the cylinders varies and it reaches a minimum at $AR = 1.5$ and it slightly increases once $AR = 2.0$. Besides, the amplitude of the fluctuating drag coefficient is larger for the upstream cylinder as compared with that of the downstream cylinder. Besides, it is found that the minimum St = 0.065 occurs at $AR = 0.25$, and it is regularly increased to the maximum value of St = 0.211 at $AR = 1.75$. A parabolic equation is deduced with high accuracy and a reasonable error of less than 1.8% to show the relationship between St and *AR*.

Keywords Tandem elliptic cylinders · Hydraulic diameter · Vortex shedding · Aspect ratio · Pressure distribution · Wake structure

List of Symbols

Latin alphabet

a_n	Horizontal radius of the ellipse
A	Area of the cross section
b_n	Vertical radius of the ellipse
C_D	Drag coefficient
C_{lf}	Fluctuating lift coefficient
C_P	Pressure coefficient
d_h	Hydraulic dimension
D	Diameter of the cylinder
e	Error
f	Shedding frequency
G	Gap between tandem cylinders
H	Vertical length of CFD domain
L	Length between the center of the cylinders
n	Stands for integer value (1 and 2)
P	Dynamic pressure
P_w	Wetted perimeter of the upstream cylinder
Re	Reynolds number
St	Strouhal number
t	Time
Δt	Time step
U	Freestream velocity
v	Local cross-stream velocity

Geek alphabet

μ	Dynamic viscosity of the fluid
ρ	Density of the fluid

Technical Editor: Daniel Onofre de Almeida Cruz.

✉ Javad Farrokhi Derakhshandeh
javad.farrokhi@aum.edu.kw

[1] College of Engineering and Technology, American University of the Middle East, Kuwait City, Kuwait

Acronym

AR	Aspect ratio
CFD	Computational fluid dynamics
CFL	Courant–Friedrichs–Lewy number
FVM	Finite volume method
FFT	Fast Fourier transform
MR	Mesh resolution
NS	Navier Stokes
NEC	Normal elliptic cylinder
TS	Transverse spacing
PEC	Parallel elliptic cylinder
VKS	Von Karman Street
VIV	Vortex-induced vibration
Superscript (*)	Stands for dimensionless parameters
Superscript (–)	Stands for mean parameters
Subscript (min)	Stands for minimum
(x, y)	Cartesian coordinate system
(i, j)	Directions in "x" and "y

1 Introduction

Laminar flow past tandem circular cylinders has been the subject of many studies due to the wide range of its applications. This typical arrangement can be widely applied in engineering problems, which are not limited to flow over buildings, heat exchangers and cooling systems, marine risers, pipelines lay on the sea-bed, offshore structures, and even electronic chips on the mainboard.

Useful correlations between vortex frequency and aerodynamic instabilities are available in the literature for tandem circular cylinders. Nevertheless, a satisfactory study of the flow structure concerning the fluidic parameters of two tandem elliptical cylinders has not yet been reached in detail. In this study, numerical investigations are performed over tandem elliptical cylinders. The flow structure, the location of the separation on the upstream cylinder, the characteristics of the flow such as the drag and lift coefficients, and the Strouhal number are deeply investigated.

Notably, it is considered how the frequency of the vortices alters and affects the wake structure of the downstream cylinder. It has been shown that the flow around tandem cylinders highly depends on not only the spacing ratio between the centers of the cylinders [1–7] but also the cross section shape of the cylinder [8–15]. Zdravkovich [3] observed three regimes based on the spacing between the cylinders' centers ratio (here, for two circular cylinders, $L^* = L/D_1 = L/D_2$). The first regime or overshoot was identified when the spacing between the centers of the cylinders was $L^* < 1.2$. Because of a small spacing ratio, the generated positive and negative upstream vortices are stagnant between the cylinders. While L^* was set to $1.2 < L^* < 3.5$, the second regime known as the reattachment regime can be effortlessly developed. In this condition, the generated upstream vortices have a chance to reattach the downstream cylinder. Finally, Zdravkovich [3] found by setting centers of the cylinder in $3.5 < L^* < 4$, the co-shedding regime can be created, in which the upstream vortices are only rolled into the gap between the cylinders. Later, these regimes were identified, confirmed, and even subcategorized in more regimes by other scholars [4, 16–22]. Numerical results of Alam [22] indicated that when the spacing ratio is set to $3.75 \leq L^*$, the frequency of vortices increases and the Strouhal number (St) sharply jumps from 0.12 to 0.175. The spacing ratio $L^* = 4$ plays a significant role not only in the dynamic behavior of the upstream vortices but also in generating different flow regimes. Therefore, $L^* = 4$ is chosen in this study to investigate the flow structure around the tandem elliptical cylinders.

Considering the cross section of the cylinders, in general, the geometry of cylindrical structures vary, and they can be aerodynamically categorized into three primary geometry [14, 23]: (1) circular and elliptical cylinders with a rounded surface, in which the flow separation may oscillate over a segment of the cylinder's surface, and it is not fixed; (2) sharp-edged surfaces with a fixed flow separation point; (3) combination of both geometries (1) and (2), such as D-shape cross-sectional structures. Though circular cylinders [24–31] and sharp-edged cylinders [12, 15, 32–40] have received much attention in the literature, the studies of flow structure over elliptical [11, 41–47] and D-shape structures [9, 48, 49] are limited to fewer examinations.

The flow past tandem cylinders with sharp edges such as square have been studied in great detail due to their relevance to a wide range of engineering applications [50–52] and less attention has been received for tandem rectangular cylinders [53, 54]. It has been shown by Derakhshandeh and Alam [14] and Chatterjee and Amiroudine [52] that the vortex structure in the wake of the cylinders with sharp edges behaves differently as compared with tandem circular cylinders. One of the main reasons is related to the fact that the cylinders with sharp edges have a fixed stagnation point causing differences in critical regimes. The separation mechanism in tandem square cylinders alters the vortex frequency at a range of Re = 55–60 due to the change of flow pattern in the wake of the tandem cylinders. The numerical studies performed by Sohankar and Etminan [51] showed that by increasing Re, the drag coefficient of the upstream square cylinder remains constant while that of the downstream cylinder gradually increases due to the altering the flow structure in spacing between the cylinders.

Using elliptical structures, on the other hand, is becoming more common these days due to their structural strength [45]. Since the flow over the elliptical cylinders can be affected by geometrical parameters such as Aspect Ratio ($AR = a_1/b_1$ see Fig. 1) and the angle of attack of the elliptical

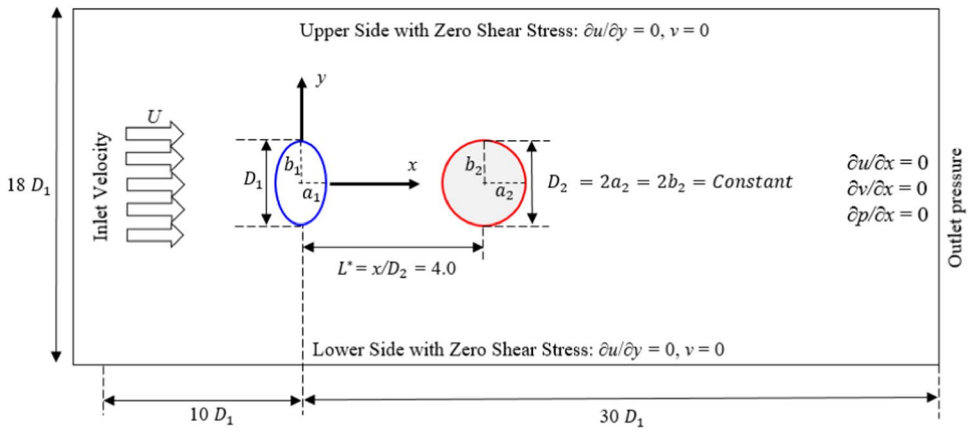

Fig. 1 Schematic of the flow past a tandem elliptical cylinders, including the computational domain and the boundary conditions

cylinder, the wake structure of vortices become more complex as compared with tandem circular cylinders. Here, a_1 and b_1 are defined as the parallel and normal radiuses of the cross section of the elliptic cylinder relative to the freestream velocity.

Flow over a normal and parallel elliptic cylinder to the flow was studied by Johnson et al. [41] and Raman et al. [46], respectively. The selected *AR* in both studies was $0 < AR < 1.0$. While Johnson et al. [41] selected a smaller range of Reynolds numbers, e.g., $30 < Re < 200$ in their studies, Raman et al. [46] focused on a relatively wider range of Re ($50 < \mathrm{Re} < 500$). Here, $\mathrm{Re} = \rho U d_h / \mu$, where ρ and U are the density and velocity of the fluid, d_h stands for the hydraulic diameter and μ represents the dynamic viscosity of the fluid. Johnson et al. [41] in their numerical studies found that for the *Normal Elliptic Cylinder* (*NEC* or with 90° incidence) by decreasing *AR*, the vortex shedding in the wake of the elliptical cylinder occurs differently as compared with von Karman Street (VKS) of a single circular cylinder. Two distinct regions behind the elliptic cylinder were identified. The first region appeared with two expanded rows of vortices, where the vortices rolling up from each side of the cylinder's surface. The vortices were placed around the second region with fairly dead dynamic vortices in between when $AR = 0.5$ at $\mathrm{Re} = 40$. It was also observed that the drag coefficient increases by increasing the Re for all aspect ratios except $AR = 1$ [11]. Since the viscous drag acts parallel to the bluff body, they showed that when Re increases, the pressure drag also increases up to 25% depends on *AR*. The results revealed that for all *AR* of test cases, the viscous drag is smaller than that of a circular cylinder since it acts normal to the surface. In the meantime, it was found that the pressure drag is more significant due to its action, which is normal to the surface of the NEC. Even though impressive results were found in this study, the hydraulic diameter of the elliptical cylinder was approximated by the vertical diameter of the ellipse ($2\ b_1$), which was not precise enough.

On the other hand, the flow over a parallel elliptic cylinder (*PEC* or with 0° incidence) was investigated by Raman et al. [46]. The results showed that by increasing *AR*, the drag coefficient increases while it decreases with increasing Re. The vortex frequency values also decrease with increasing *AR*; however, these vortex shedding frequencies can increase from 0.165 to 0.23 when the Re number grows from 100 to 500. Though the Re was relatively higher than the selected range of Re by Johnson et al. [11], a 2D numerical in-house code was used to investigate the flow features. As the 3D vortex structure can be generated for $\mathrm{Re} > 200$, using a 2D code might correlate with some errors [33, 55]. In addition, the details of the evaluation of the length scale of the elliptical cylinder have been not provided in their study [46]. The dynamic response of the elastically mounted elliptical cylinder was studied at different angles of attack by Leontini et al. [56]. Though different flow regimes were observed by authors once the angle of attack changed, the hydraulic diameter of the elliptical cylinder was simply chosen as the length scale for evaluating Re [56].

The effect of *AR* on the flow past an elliptical cylinder was also examined by Faruquee et al. [42] at zero incidences, where the major axis of the elliptic cylinder was parallel to the flow stream. A series of test cases were chosen and examined with $0.3 < AR < 1$ at $\mathrm{Re} < 40$. The numerical results showed that at a very low range of *Re* (e.g., $5 < \mathrm{Re} < 10$), a pair of steady vortices generates in the wake of the cylinder when the critical aspect ratio was $AR = 0.34$. For smaller *AR*, no significant vortices were shed in the wake of the cylinder. They also observed that when $AR < 0.6$, the viscous forces become more dominant, while for $AR > 0.6$, the pressure forces become more influential.

Later, Vijay et al. [57] numerically studied the effect of *AR* on flow-induced vibration of the elliptical cylinder with a constant mass ratio of 10 when $\mathrm{Re} = 100$. The authors showed

that a synchronization regime is directly correlated with aspect ratio, and found that lock in response occurs for small aspect ratios and the magnitude of oscillation of elliptical cylinder with $AR = 0.1$ is twice that of a circular cylinder Vijay et al. [57]. While 2 single vortices (2S mode) were observed in this study for all examined aspect ratios, the Reynolds number was set based on the major axis with the elliptical cylinder.

2D numerical simulations were performed by Nair et al. [58] to study the influence of a wall on the wake structure of circular and elliptical cylinders. Nair et al. [58] examined different gaps between cylinder and wall, which was set between 0.1 and 1.0 with Re = 40–1000. In this study, the diameters of circular and elliptical cylinders were considered for evaluating Re. Thus, the results of circular and elliptical cylinders did not show significant changes due to the geometrical parameters, when an identical gap and diameter were used in simulations [58].

The literature review given above demonstrates that both the spacing between the centers of the tandem cylinders and the cross section area of the cylinders are two critical parameters that remarkably affect the Karman vortex structure and imposed forces on the cylinders. To the authors' knowledge, there has been no prior study on the flow over tandem elliptical cylinders to examine the effect of the aspect ratio of the upstream cylinder on the wake structure. Besides, in the majority of the previous studies, the Reynolds number length scale was only identifiable with $D_1 = 2b_1$ (see Fig. 1). The previously published studies neither considered the wet perimeter of the elliptical cylinder nor provided the details of explanation for evaluating accurate hydraulic diameter.

According to the above gap in the literature, in this study, we attempt to evaluate and use the precise hydraulic diameter of the elliptical cylinder using the Ramanujan approximation theorem, which has not been used before in literature. Based on this theorem and to better understand the flow instabilities in the wake and around the cylinders, we numerically investigate the vortex shedding frequency, forces (lift and drag) coefficients of the cylinders once the aspect ratio of the upstream cylinder alters from *VEC* (with 90° incidence) to *PEC* (with 0° incidence).

2 Mathematical equations and numerical model

The Navier–Stokes (*NS*) equations in two dimensions are used for incompressible laminar viscous flow. The conservation of mass can be given as:

$$\frac{\partial u_i}{\partial x_j} = 0. \tag{1}$$

The conservation of the momentum can be written as:

$$\frac{\partial u_i}{\partial t} + u_j \frac{\partial u_i}{\partial x_j} = -\frac{1}{\rho}\frac{P}{x_i} + \frac{\partial}{x_j}\left(\vartheta \frac{\partial u_i}{\partial x_j}\right). \tag{2}$$

In the above equation, u (x, y, t) and P (x, y, t) are the velocity and pressure fields of the fluid in "i" and "j" directions. Considering the Eulerian solution of the *NS* equations, the finite volume method (FVM) was used in ANSYS Fluent software to simulate the test cases. The governing equations of fluid flow, thus, were integrated and solved iteratively based on the conservation of mass and momentum on each control volume. Since FVM can be used for the structured and unstructured meshes, the structured mesh was created for all simulations. The numerical discretization was based on the second-order upwind differencing scheme to increase the accuracy of the solution. The computational domain around the cylinders is shown in Fig. 1. Water properties as a Newtonian fluid were chosen and set in the ANSYS Fluent database with a density of $\rho = 998.2$ (kg/m3) and the dynamic viscosity of $\mu = 0.001003$ (Pa. s). In the simulations, the flow on the surfaces of the cylinders was set with zero velocity and no-slip.

The aspect ratio of the upstream cylinder varies from $AR = 0.25$ to 2.0. Therefore, the maximum and minimum gap ratio of $G^* = G/D_2 = 3.375$ and 2.5 were produced, respectively, and accordingly, eight configurations were modeled and studied as shown in Fig. 2. The advantage of this selection is examining both NEC and PEC in a tandem arrangement of the cylinders. Figure 2 highlights the variation of AR of the upstream cylinder in pink dash-lines. The thicker pink dash-lines highlight the minimum and maximum aspect ratios, whereas the blue dash-line shows the elliptic cylinder with $AR = 1.0$ or a simple circular cylinder. The hydraulic diameter of the upstream cylinder is considered for evaluating the Re. By using different AR, the hydraulic diameter of the upstream cylinder changes due to the alteration of area and perimeter. Consequently, it is important to note that Re should be evaluated and set at Re = 200 separately for each model based on the new hydraulic diameter (d_h) of the upstream cylinder. For each test case, d_h is calculated using the following formula:

$$d_h = \frac{4A}{P_w}. \tag{3}$$

Here A represents the cross-sectional area of the elliptical upstream cylinder and P_w stands for the wetted perimeter of the cylinder. Though the area of the elliptical cylinder can be calculated accurately based on the major and minor axes of the ellipse, e.g., $A = \pi a_1 b_1$, the perimeter of the elliptical cylinder is challenging to be accurately calculated [59]. There are many theorems and formulas to estimate the cross-sectional perimeter of the elliptic cylinder, such as the Ramanujan approximation theorem and Maclaurin

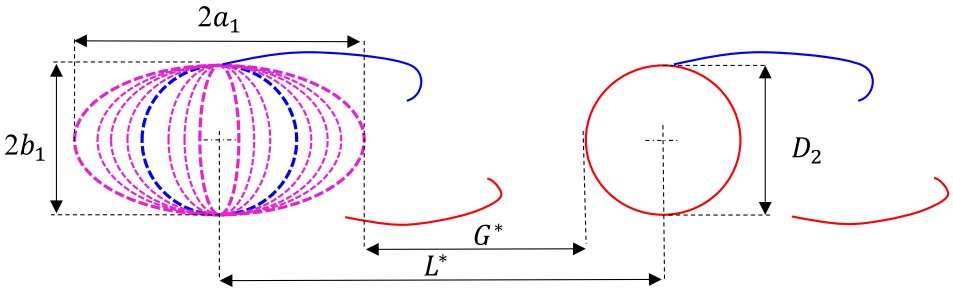

Fig. 2 Schematic of tandem elliptical cylinders showing the variation of the aspect ratio of the upstream cylinder in dash lines. The blue dash-line highlights the $AR=1$ (simple circular cylinder). The spacing ratio between the centers of the cylinders is L^*, while G^* is the gap ratio between the cylinders; the AR of the downstream cylinder was kept constant in all test cases. The thicker pink dash-lines of the upstream cylinder highlights the minimum and maximum AR corresponding to the normal and parallel elliptic cylinders to the flow, respectively

expansion [59, 60]. Ramanujan approximation theorem with high accuracy is one of the acceptable theorem, which can be used with an excellent satisfactory error ($e<10^{-2}\%$) to estimate the perimeter of the elliptic cylinder. The Ramanujan approximation is given by:

$$P_w = \pi\left[(a_1+b_1)+\frac{3(a_1-b_1)^2}{10(a_1+b_1)+\sqrt{a_1^2+14a_1b_1+b_1^2}}+e\right] \quad (4)$$

Table 1 summarizes the geometrical parameters of the upstream elliptical cylinder, comprising the parallel and normal radiuses, and the area and perimeter and the hydraulic diameter of the upstream cylinder. In 2D modeling, the length of the cylinder is set to one in all simulations. It is observed that by changing the aspect ratio, both the cross section area and wetted perimeter of the upstream cylinder change. These two aspects directly affect the hydraulic diameter of the cylinder. Hence, the last column of the table shows the hydraulic diameter of the cylinder, which is used for evaluating Re.

Table 1 The geometrical parameters of the upstream elliptic cylinder to evaluate the hydraulic diameter of the elliptical cylinder

Test case	a_1 (mm)	b_1 (mm)	AR	G^*	Area (mm^2)	Perimeter (mm)	d_h (mm)
1	6.25	25.00	0.25	3.375	490.25	107.23	18.31
2	12.50	25.00	0.5	3.250	981.25	121.10	32.42
3	18.75	25.00	0.75	3.125	1471.87	138.14	42.63
4	25.00	25.00	1.0	3.000	1962.50	157.08	50.00
5	31.25	25.00	1.25	2.875	2453.12	177.26	55.38
6	37.50	25.00	1.5	2.750	2943.75	198.31	59.40
7	43.75	25.00	1.75	2.625	3434.37	220.02	62.46
8	50.00	25.00	2.0	2.500	3925.00	242.21	64.85

Table 2 Estimation of the error by assuming that the hydraulic diameter of the elliptic cylinder is identical with the diameter of a circular cylinder

AR	$d_{h,ellipse}=\frac{4A}{P_w}$	$Re=\rho U d_{h,ellipse}/\mu$	$D_{h,circle}=\frac{4A}{P_w}$	$Re=\rho U D_{h,circle}/\mu$	Error%
0.25	18.31	200	50	546.1	177.6
0.50	32.42	200	50	308.5	54.2
0.75	42.63	200	50	234.3	17.1
1.00	50.00	200	50	200	0
1.25	55.38	200	50	180.6	9.6
1.50	59.40	200	50	168.1	15.9
1.75	62.46	200	50	160.2	19.8
2.00	64.85	200	50	154.2	22.8

It is worth estimating the percentage of the discrepancy (or error) for the hydraulic diameter if the Reynolds number length scale was identical with a diameter of a circular cylinder. Considering the hydraulic diameters of a circle and an ellipse, (e.g., $D_{\mathrm{h,circle}}$ and $d_{\mathrm{h,ellipse}}$, respectively), the accurate amount of Re for the circular cylinder ($\mathrm{Re_c}$) can be estimated according to the following equation:

$$\mathrm{Re_c} = \mathrm{Re_e} \times \frac{D_{\mathrm{h,circle}}}{d_{\mathrm{h,ellipse}}} \tag{5}$$

Table 2 comprises two Reynolds numbers that can be calculated based on the precise hydraulic diameter of the elliptic cylinder using the Ramanujan formula or an estimated diameter of a simple circular cylinder. The last column of the table displays the percentage of the error between the accurate value and estimation one. The results show that nonlinear error is obtained for calculating Re resulting in a larger error for the NEC as compared with the PEC. To provide a clearer prospect, the amount of error versus *AR* is shown in Fig. 3, which is associated with Table 2. It is found that even for a relatively low Re, the maximum error for evaluating Re, approximately reaches 178% and 25% for NEC and PEC, respectively. The amount of error is calculated based on the following equation:

$$\mathrm{Error} = \frac{\left(D_{\mathrm{h,circle}} - d_{\mathrm{h,ellipse}}\right)}{d_{\mathrm{h,ellipse}}} \times 100(\%) \tag{6}$$

Therefore, to avoid these errors and study the flow structure of elliptical cylinders with high accuracy and reliability,

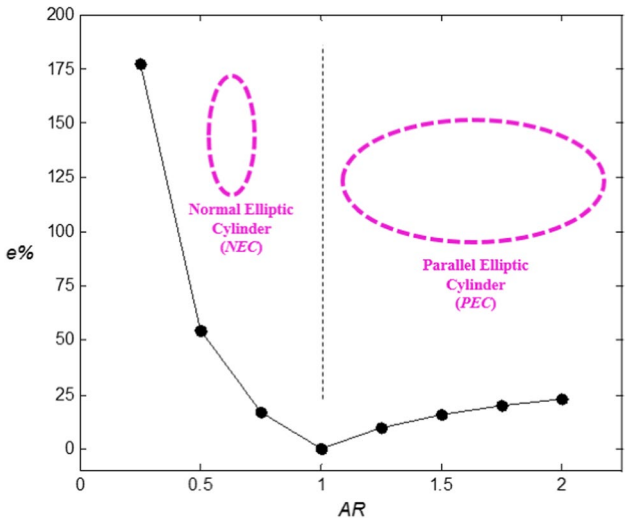

Fig. 3 Variation of the percentage of error as a function of *AR* at Re = 200 when the hydraulic diameter of the elliptic cylinder is evaluated by the diameter of a circular cylinder. The data are associated with Table 2

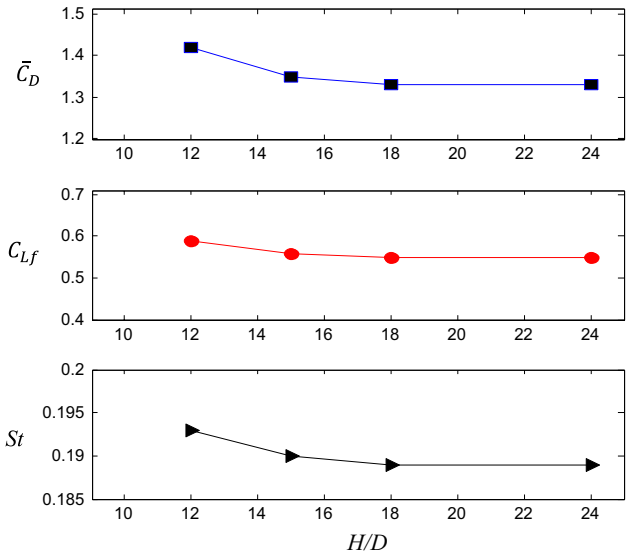

Fig. 4 Effects of blockage on the mean-drag coefficient, the fluctuating lift coefficient and the Strouhal number of the upstream cylinder arranged in a tandem elliptical cylinders with *AR* = 1 (circular cylinder) at Re = 200

here the Ramanujan approximation is used to evaluate the perimeter of the elliptical cylinder, and consequently, hydraulic diameter of the cylinder.

In numerical simulations, to avoid the blockage effects, four computational widths were selected and set at $H/D_1 = 12$, 15, 18, and 24 for a typical tandem circular cylinders (when $AR = 1$ for both cylinders) at Re = 200. Figure 4 shows the effect of blockage on the mean drag coefficient as well as fluctuating lift coefficient and Strouhal number of the upstream cylinder. Though it is seen that there is about 2% discrepancy between $H/D_1 = 15$ and 18, the results reveal that by increasing the width to 18, the trends of $\overline{C}_{\mathrm{D}}$, C_{lf}, and St remain constant. Thus, the computational width with $H/D = 18$ is chosen for the rest of the simulations.

The upstream and downstream lengths of $10D_1$ and $30D_1$ are also selected for the total length of the domain. These distances are long enough to guarantee that the inlet and outlet effects are eliminated [61–64]. Here, D_1 is the vertical length of the upstream cylinder and is kept constant and equal to $D_1 = 2b_1 = 2b_2 = D_2$ in all test cases. Consequently, the *AR* was varied only by altering the horizontal axis of the cylinder (e.g., a_1).

3 Results and discussion

In this section, the numerical simulation is initially validated. Then, the flow structure in the wake of the cylinders and fluidic parameters such as pressure coefficients, and the lift and drag coefficients are analyzed in detail. Finally, the

Table 3 Mesh resolution independence results at Re = 200, including the mean-time drag coefficients and the fluctuating lift coefficients of the cylinders and the Strouhal number of the upstream cylinder at $AR = 1$

Fluidic parameters	Number of grids		
	$MR_1 = 34{,}822$	$MR_2 = 46{,}256$	$MR_3 = 61{,}366$
$\overline{C}_{D(1)}$	1.189	1.440	1.460
$\overline{C}_{D(2)}$	0.31	0.35	0.36
$C_{lf(1)}$	0.544	0.553	0.553
$C_{lf(2)}$	1.105	1.118	1.119
$St_{(1)}$	0.171	0.174	0.175

effect of aspect ratio on the Strouhal number is studied, and a relationship between AR and St is derived.

3.1 Verification

To test the grid independence, three structured mesh resolution namely: MR_1, MR_2 and MR_3 were examined for the flow over tandem circular cylinders. The results of each test are summarized and compared in Table 3, comprising the mean-time drag coefficient of the cylinders ($\overline{C}_{D(1)}$ and $\overline{C}_{D(2)}$) the fluctuating lift coefficient of the cylinders ($C_{lf(1)}$, and $C_{Dlf(2)}$) and St. A typically generated mesh in the flow domain and around tandem elliptical cylinders are shown in Fig. 5, when the aspect ratio of the upstream and downstream cylinders are set at $AR = 0.25$ and 1.0, respectively.

It is worth noting that similar to the previously published data [22], the Strouhal number was identical for both circular cylinders, and therefore, one value is only presented in Table 3. The minimum mesh size in the finest mesh resolution (e.g., MR_3) was approximately 0.02. Based on this size, the time step of $\Delta t = 0.025$ (s) was chosen, which was adequately small to satisfy the Courant–Friedrichs–Lewy number ($CFL = U\Delta t/\Delta x < 1$). The results of Table 3 highlight that MR_2 is an acceptable mesh resolution as compared with MR_3. While the maximum error of $e_{C_{D(1)}} \approx 4\%$ was obtained for the drag coefficient of the upstream cylinder, other parameters show less than 2% errors. Therefore, MR_2 was selected for the rest of the numerical simulations.

Further validations were also conducted for flow over tandem circular cylinders at Re = 200. Table 4 compares the obtained numerical results including $\overline{C}_{D(1)}$, $\overline{C}_{D(2)}$, $C_{lf(1)}$, $C_{Dlf(2)}$, and St with those in literature. The subscripts '1' and '2' in Table 3 refer to the upstream and downstream cylinders, respectively. It is seen that the present results are in good agreement with published data. While the percentage

Table 4 Comparison between the fluidic parameters comprising drag coefficients, fluctuating lift coefficients, and the Strouhal number of tandem circular cylinders with $AR = 1$ at Re = 200

Scholars	$\overline{C}_{D(1)}$	$\overline{C}_{D(2)}$	$C_{lf(1)}$	$C_{lf(2)}$	St
Present study	1.332	0.591	0.559	1.385	0.189
Alam [22]	1.255	0.36	0.551	1.117	0.175
Koda and Lien [65]	1.285	0.440	0.558	1.229	0.170
Mahir and Altac [37]	1.340	0.558	0.569	1.407	0.181
Dehkordi et al. [66]	1.160	0.520	0.575	1.059	0.179

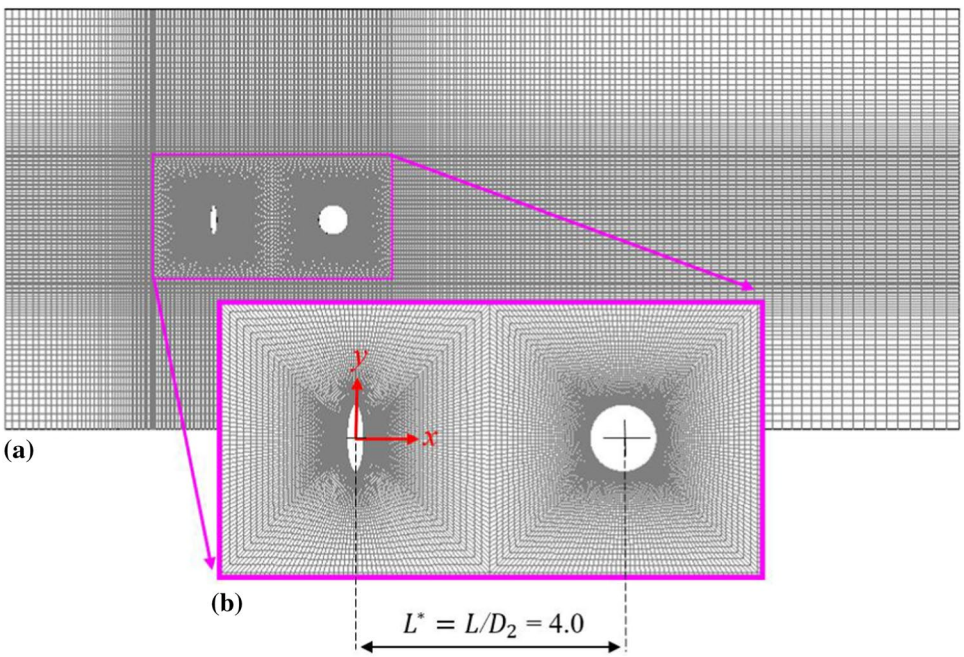

Fig. 5 A typically structured mesh around tandem elliptic cylinders, including a closer view of the grids around the cylinders, when the aspect ratio of the upstream cylinder is $AR = 0.25$

of deviation between the results is acceptable, the best match is seen between the present study and the data offered by Mahir and Altac [37] for all parameters with less than 5%.

3.2 Separation points and reattachment locations

Highlighting the details of flow separation can gain more insight into the flow structure in the wake of the upstream elliptical cylinder. The separation points also directly can affect the reattachment of vortices on the downstream cylinder. Both of these locations can influence the imposed pressure on the cylinders. Samples of instantaneous vorticity contours are shown in Fig. 6a–c at Re = 200 for three aspect ratios, minimum ($AR = 0.25$), identical ($AR = 1.00$), and maximum ($AR = 2.00$). The figure shows the separation points, separation angles, and the locations of reattachments. As is well known, the boundary layer equation is a valid approximation for a wide range of Re until separation begins to intervene. In a laminar flow, such a feature corresponds to disappearing wall shear stress when the flow is broken away from the surface of the bluff body. Accordingly, the exact separation angle (e.g., θ_S) can be extracted from numerical results, where the wall shear stress vanishes on the surface of the upstream elliptical cylinder.

Figure 6 highlights that by increasing AR, the separation points shift to the trailing surface of the upstream cylinder and the separation angle gradually increases. On the other hand, due to the increment of separation angle at larger AR, the spacing ratio between cylinders reduces; thus, the reattachment of the vortices on the downstream cylinder also takes place at larger angles as compared to the smaller AR.

The position of separation points can be understood by choosing the peak of the distribution of the fluctuating pressure coefficient around the cylinder [67, 68]. Accordingly, the RMS fluctuation pressure coefficients of the upstream and downstream cylinders are plotted in Fig. 7 for all AR.

Figure 7 shows that the peak of $C_{Pf(1)}$ occurs at about 90° for $AR = 0.25$. The sinusoidal trend, then, is seen after a peak of $C_{Pf(1)}$. By increasing AR, the magnitude of $C_{Pf(1)}$ gradually decreases. It is also observed that the peaks shift to larger angles (larger than 90°) and relocates on the trailing surface of the upstream cylinder, which again confirms the results of vorticity contours in Fig. 6. It is observed that the sinusoidal trend of $C_{Pf(1)}$, gradually alters to one oscillation for $0.25 < AR < 1.25$ and for $AR \geq 1.25$, the curves change to a relatively flat trend. On the other hand and in general, the maximum fluctuating pressure of the downstream cylinder is $C_{Pf(2)} < 1$ for all AR. The peaks of $C_{Pf(2)}$ of $AR = 0.25$ and 0.5 occur at 68° and 60°, respectively, which are larger than that one with higher aspect ratios except $AR = 2.0$. By increasing AR to 0.75, the peak of $C_{Pf(2)}$ approximately 30% increases as compared to that of $AR = 0.5$; however, the angle of reattachment at $AR = 0.75$ shifts to a smaller angle of 46°. For

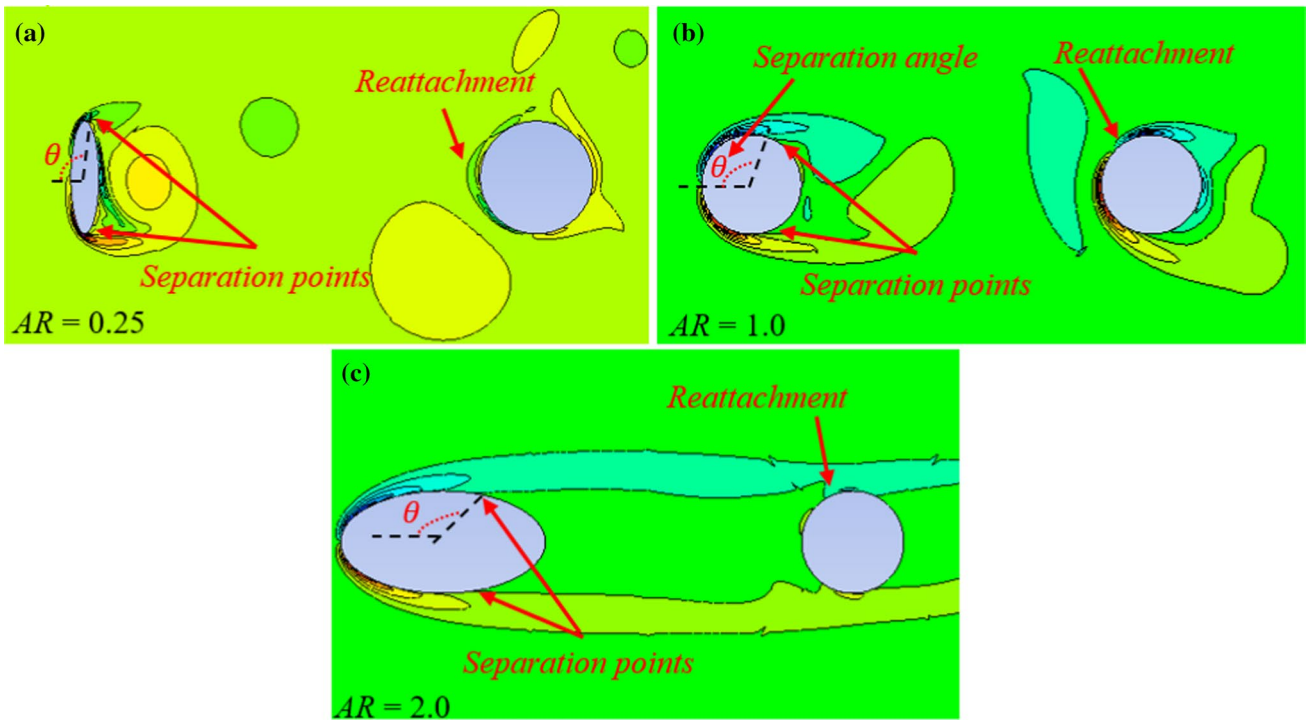

Fig. 6 Separation and reattachment points of the upstream and downstream cylinders for test cases with **a** minimum aspect ratio, $AR = 0.25$, **b** identical aspect ratio, $AR = 1.00$ and **c** maximum aspect ratio, $AR = 2.00$ at Re = 200

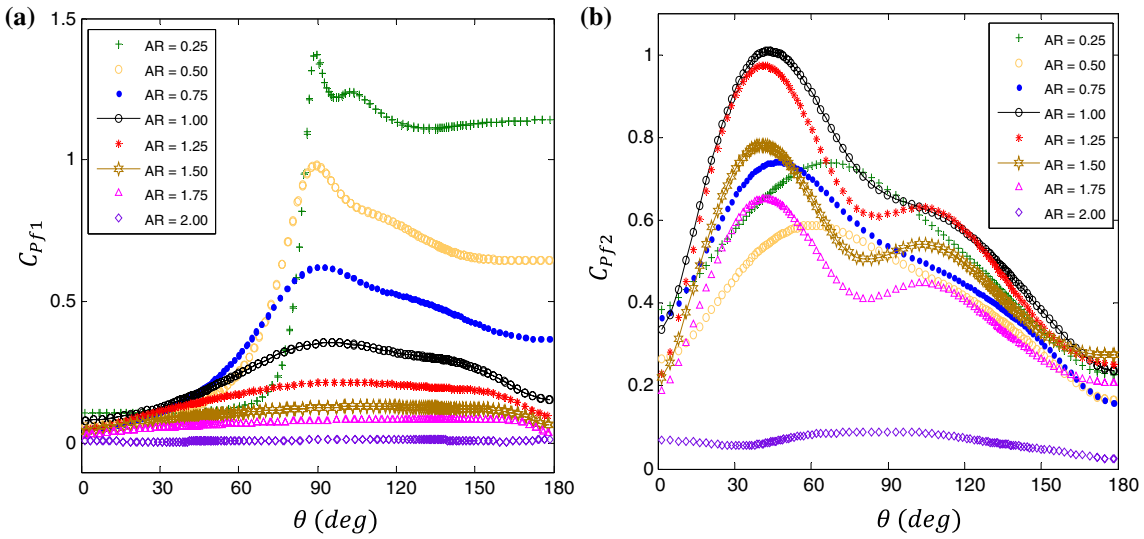

Fig. 7 Root-mean-square pressure fluctuations of **a** upstream and **b** downstream cylinders for tested cases of $AR = 0.25$ to 2.00 at $\mathrm{Re} = 200$

$AR = 1.0$ till 1.75, the peaks of $C_{\mathrm{Pf(2)}}$ are found to be about 43°, 40°, 39.5°, and 39°, respectively. For test cases with $AR > 1$, it is observed that the magnitude of $C_{\mathrm{Pf(2)}}$ gradually decreases. This means the influence of vortices becomes smaller on the downstream cylinder as compared to those with $AR < 1$. The pressure fluctuations become very low or minimum around the upstream and downstream cylinders when $AR = 2.0$. Therefore, it is expected the imposed forces on both cylinders with $AR = 2.0$ become minimum.

To gain a better understanding and insight about the pressure distribution of tandem cylinders, first, the time-averaged pressure distribution ($\overline{C}_{\mathrm{P}}$), and RMS fluctuating pressure distribution (C'_{p}) along with the single circular cylinder at $\mathrm{Re} = 200$ are both shown in Fig. 8a, b. Figure 8c also depicts the time-averaged contour plots of the pressure coefficient of the cylinder. It is seen that the maximum pressure on the single cylinder occurs at around 82°, which is consistent with the literature [68].

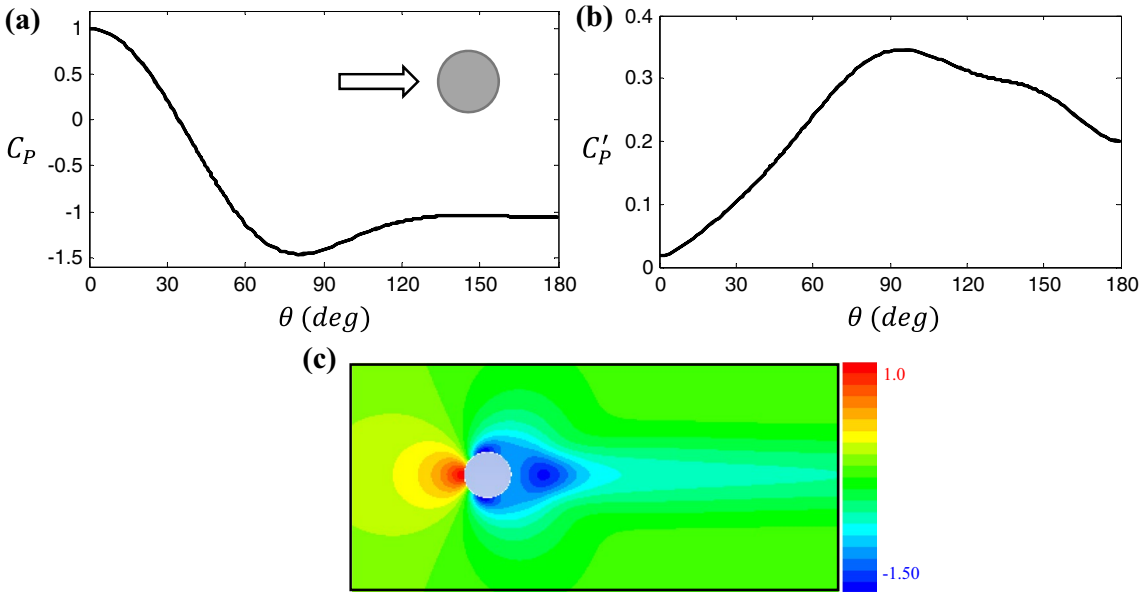

Fig. 8 Pressure coefficient distribution over the surface of a single cylinder at $\mathrm{Re} = 200$, **a** time-averaged pressure coefficient distribution ($\overline{C}_{\mathrm{P}}$), **b** RMS fluctuating pressure coefficient (C'_{p}), **c** time-averaged contour plot of pressure coefficient

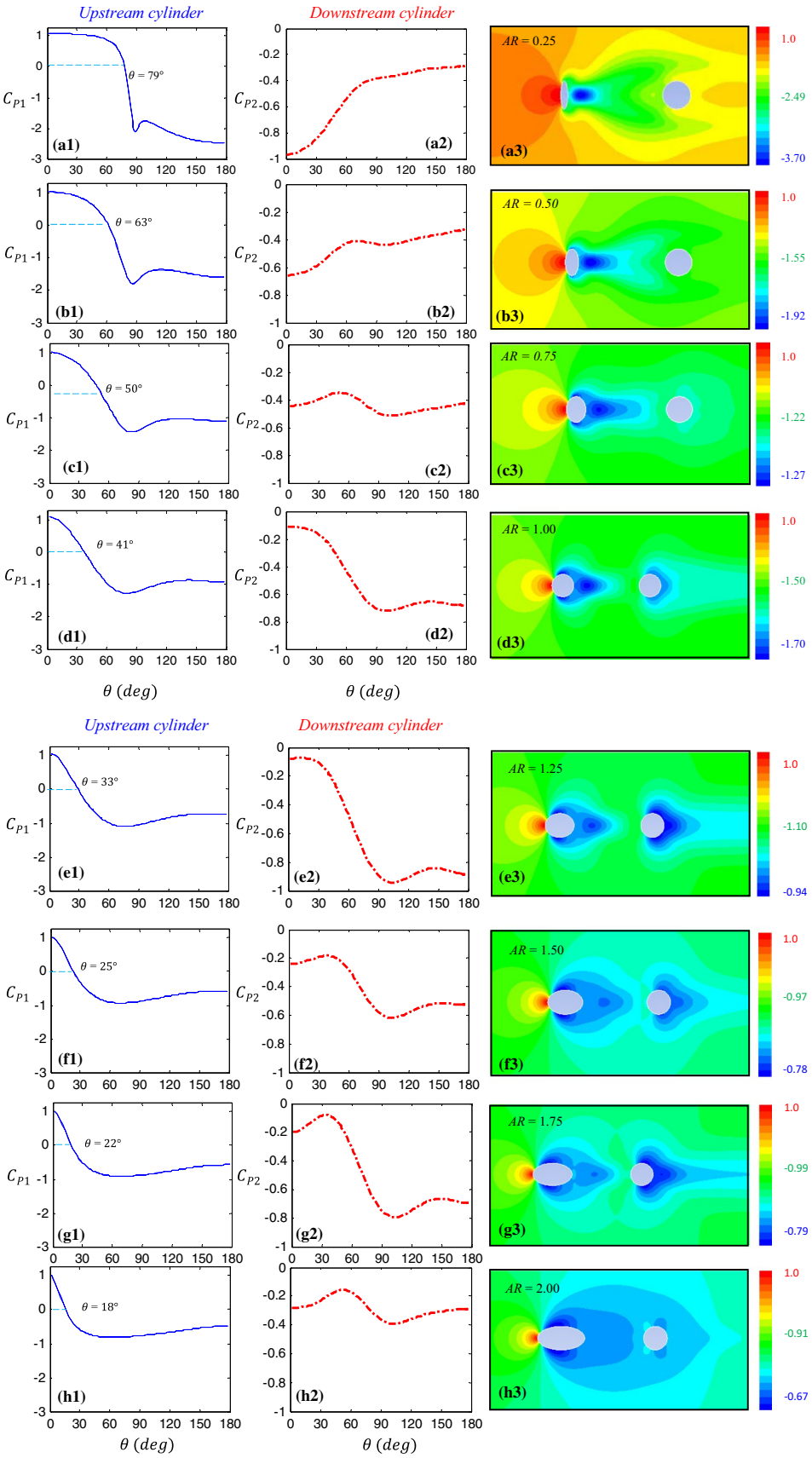

Fig. 9 Time-averaged pressure coefficient distribution along the surface (left and middle columns) and in the wake of the tandem elliptical cylinders (right column) with spacing $L^*=4$ at $\mathrm{Re}=200$ as a function of aspect ratio of the upstream cylinder, **a** $AR=0.25$, **b** $AR=0.50$, **c** $AR=0.75$, **d** $AR=1.00$, **e** $AR=1.25$, **f** $AR=1.50$, **g** $AR=1.75$, **h** $AR=2.00$

In Fig. 9, the distribution of the time-averaged pressure coefficients ($\overline{C}_P$) along the surfaces of the upstream (left column) and downstream (middle column) cylinders are presented, respectively. The right column of Fig. 9 also shows the time-averaged contour plots of the pressure coefficient in the wake area of the cylinders. On comparing Figs. 8 and 9, it is observed that except for two test cases, $AR=0.25$ and 0.5, the trend of $\overline{C}_{P(1)}$ for the rest of the models is very similar to that around a single circular cylinder. It is seen that the pressure distribution on the upstream cylinder includes positive and negative values and alters as a function of AR; however, the downstream cylinder is always in a negative region apart from the aspect ratio of the cylinders.

The positive $\overline{C}_{P(1)}$ on the upstream elliptical cylinder occurs at $\theta \leq 79°$ for $AR=0.25$. By increasing AR, the angle of positive values of $\overline{C}_{P(1)}$ on the leading edge of the elliptical cylinder gradually decreases, and therefore, $\overline{C}_{P(1)}=0$ steadily shifts to smaller angles as shown in Fig. 9. Comparison of $\overline{C}_{P(1)}$ reveals that the maximum negative magnitude of pressure coefficients of the upstream cylinder gradually decreases by increasing AR. This decrement is very sensible when AR alters from 0.25 to 0.50, in which $\overline{C}_{P(1)}$ shows 25% less pressure (e.g., $\overline{C}_{P(1)}$ changes from -2.4 at $\theta=180°$ to -1.8 at $\theta=86°$). Since, $\overline{C}_{P(1)}$ at the rear surface of the upstream cylinder for $AR=0.25$ and 0.50 is much larger as compared with other test cases, it is expected to generate a reduced drag force on the upstream cylinder for these two test cases. This concept will be explained in the next section.

On the other hand, the results of $\overline{C}_{P2}$ show that the time-averaged pressure distribution along the downstream cylinder is not similar to that around a single nor upstream one. The values of $\overline{C}_{P(2)}$, in general, are negative and smaller than that of the upstream cylinder (Fig. 9) or the single cylinder (Fig. 8a). It is found that, for $AR>0.75$, in which the gap between cylinders reduces, the maximum negative magnitude of $\overline{C}_{P(2)}$ occurs after $\theta=90°$ as it was expected earlier due to the reattachment. The contour plots in the wake and around the cylinders confirm that at $AR=0.25$ and 0.5, the pressure distribution corresponds to larger negative values of $\overline{C}_P$ on the lower and upper sides of both cylinders and in the wake of the upstream cylinder.

The contour plots of Fig. 9 also show that the minimum time-averaged pressure coefficient over the surface of the cylinder occurs at smallest $AR=0.25$ with the magnitude of $\overline{C}_P=3.7$. Further increasing in $AR=0.5$, the magnitude of $\overline{C}_P$ shows a sudden drop to 1.92 on the cylinder surface and $\overline{C}_P$ regularly decreases to the minimum magnitude of $\overline{C}_P=0.82$ for the largest $AR=2.00$. To better understand the discrepancy of the $\overline{C}_P$ in the wake of tandem cylinders, the variation of $\overline{C}_{P,min}$ versus to the AR is plotted in Fig. 10.

3.3 Lift and drag coefficients

Figure 11 shows the time history of the lift coefficients of the upstream elliptical cylinder and downstream circular cylinder at different AR (left column). The figure also represents the Fast Fourier transform (FFT) function corresponding to the peaks of the lift coefficient of the upstream cylinder over the total convergence time (right column).

The time history of the lift coefficients can be considered in terms of the amplitude of the forces and phase lags between the forces. As expected in the previous section, the magnitude of the lift coefficient shows the maximum value when $AR=0.25$, and it reaches a minimum value at $AR=2.0$. The results also reveal that the phase lag between the sinusoidal lift coefficients of the cylinders varies by changing AR and it gradually reduces. The phase lag reaches

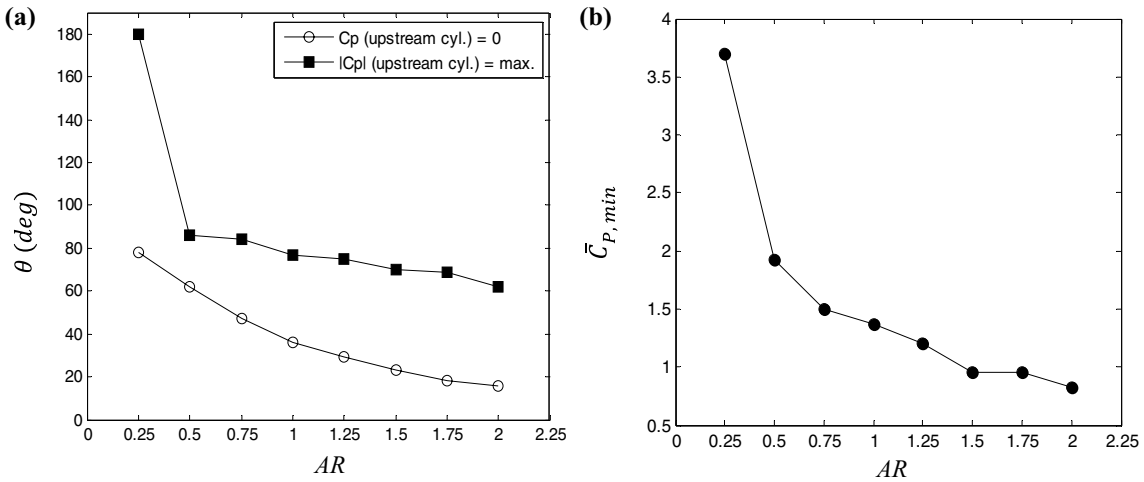

Fig. 10 **a** Different angles of upstream elliptical cylinder where the magnitude of $\overline{C}_P$ becomes maximum and zero, **b** variation of $\overline{C}_{P,min}$ as a function of AR for the upstream cylinder extracted from contour plots of Fig. 9 (a_3–h_3)

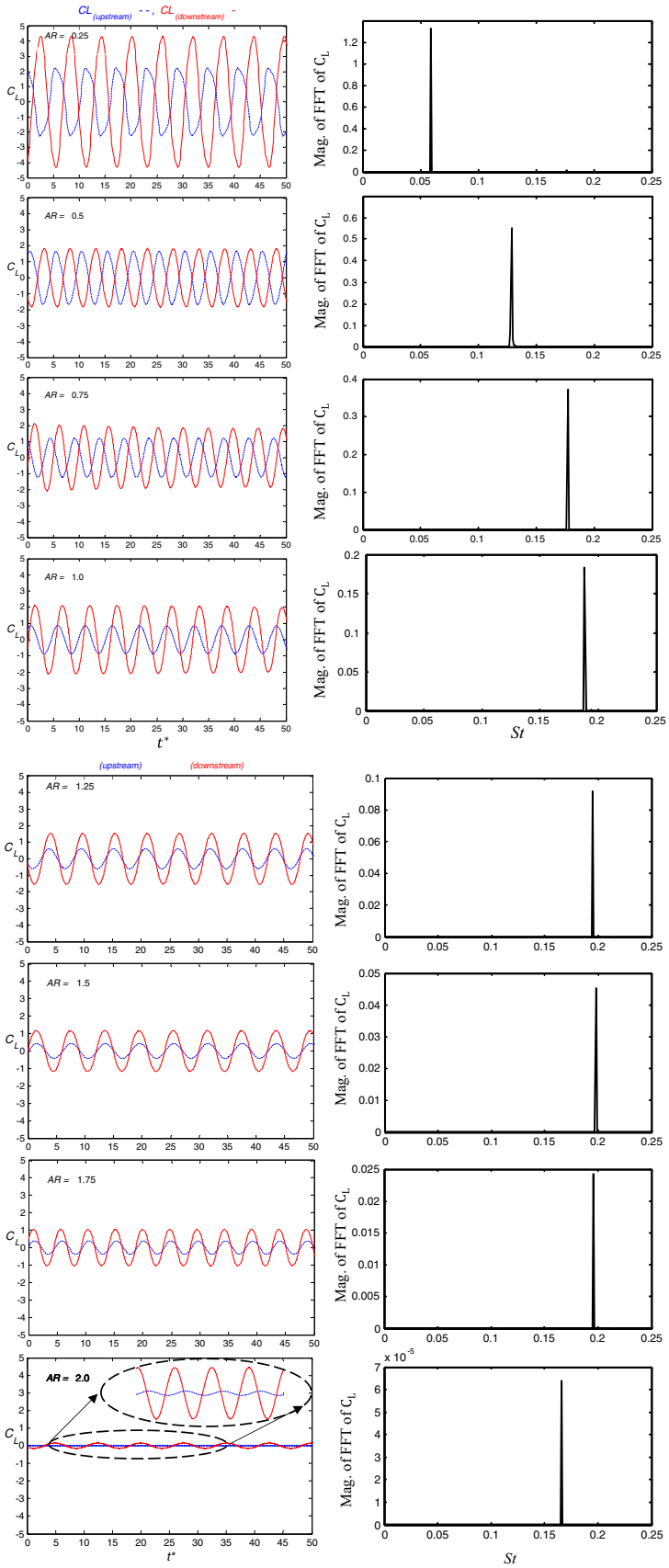

Fig. 11 Time history of the lift coefficients of the upstream elliptic cylinder and downstream circular cylinder with different *AR* (left column) and the magnitude of FFT of the lift coefficient showing the Strouhal number (right column)

a minimum at $AR = 1.5$ and it increases again by an increment of AR to 2.0. When comparing the FFT figures for each AR it becomes readily apparent that the frequency of vortices also varies. The minimum St occurs at $AR = 0.25$, and it is regularly increased to the maximum value at $AR = 1.75$. The results show that St becomes close to the vortex frequency formation of a single cylinder when $1.25 \leq AR \leq 1.75$ (e.g., St ≈ 0.2). At this range of AR (e.g., $1.25 \leq AR \leq 1.75$) the phase lags between lift forces are 14.08°, 9.98° and 27.9°, respectively. When AR increases to 2.0, vortex shedding frequency with 15% drops reaches to St = 0.17. The reason is due to the minimum gap ratio between the cylinders, which generates the overshoot regime, and hence, the vortices cannot be produced in the wake of the upstream cylinder and accelerated to increase St. It is emphasized that the overshot regime generates once the $G^* < 1.2$, where the separated shear layers of the upstream cylinder overshoot the downstream one and rolling in the wake of the downstream cylinder without reattaching [31]. The FFT plots of the lift coefficients also demonstrate that the magnitude of the lift forces is different and it varies by AR. Considering the magnitude of the FFT plots, it is confirmed that the maximum and minimum magnitude of the lift forces occur at $AR = 0.25$ and 2.0, respectively.

Table 5 Lift and drag coefficients of tandem elliptic cylinders at $Re = 200$

Test case	AR	$C_{lf(1)}$	$C_{lf(2)}$	$\overline{C}_{D(1)}$	$\overline{C}_{D(2)}$
1	0.25	1.4367	2.7623	6.8831	−1.3455
2	0.50	0.9373	1.1538	2.7991	−0.3003
3	0.75	0.6202	1.0855	1.6592	0.1288
4	1.00	0.5598	1.3857	1.3322	0.5915
5	1.25	0.3898	1.0076	1.0487	0.7668
6	1.50	0.1874	0.5413	0.8508	0.3478
7	1.75	0.1403	0.4123	0.7277	0.2655
8	2.00	0.0077	0.0929	0.6555	0.0840

The exact values of fluctuating lift coefficients (C_{lf}) and the time-averaged drag coefficients ($\overline{C}_D$) are shown in Table 5 for each test case. To better understand the trend of variation of the imposed forces on the cylinder, the fluctuating lift, and drag coefficients are plotted in Fig. 12. The results at $AR = 0.75$ and 1 are well matched with those measured and reported by Alam et al. [16]. In general, the results of the lift coefficients reveal that the upstream cylinder undergoes a smaller C_{lf} as compared with the downstream cylinder. The fluctuating lift coefficient of the cylinders follows similar trends as the spacing is increased. The fluctuations are remarkably large at $AR = 0.25$. The fluctuations of elliptical upstream cylinder remain extremely high, when $G^* = 3.375$ (e.g., $AR = 0.25$). As this gap ratio, $C_{lf(1)}$ and $C_{lf(2)}$ are 2.15 and 1.11 ($C_{lf(1)}$ 30 times higher than that of minimum G^* (test case 8), respectively (see Table 5). Although the fluctuations of the lift coefficient of both cylinders become low as the gap ratio decreases, the trend of the reduction is not similar. The variation of the $C_{lf(1)}$ is sinusoidal with a significant reduction, in particular, when AR increases to 0.5. $AR = 1.0$ can be nominated as a critical aspect ratio (AR_C), in which the fluctuating lift and drag coefficients of the downstream cylinder shows a peak. The results confirm that both C_{lf} downstream and C_{Df} upstream cylinders are very sensitive when $AR < 1$.

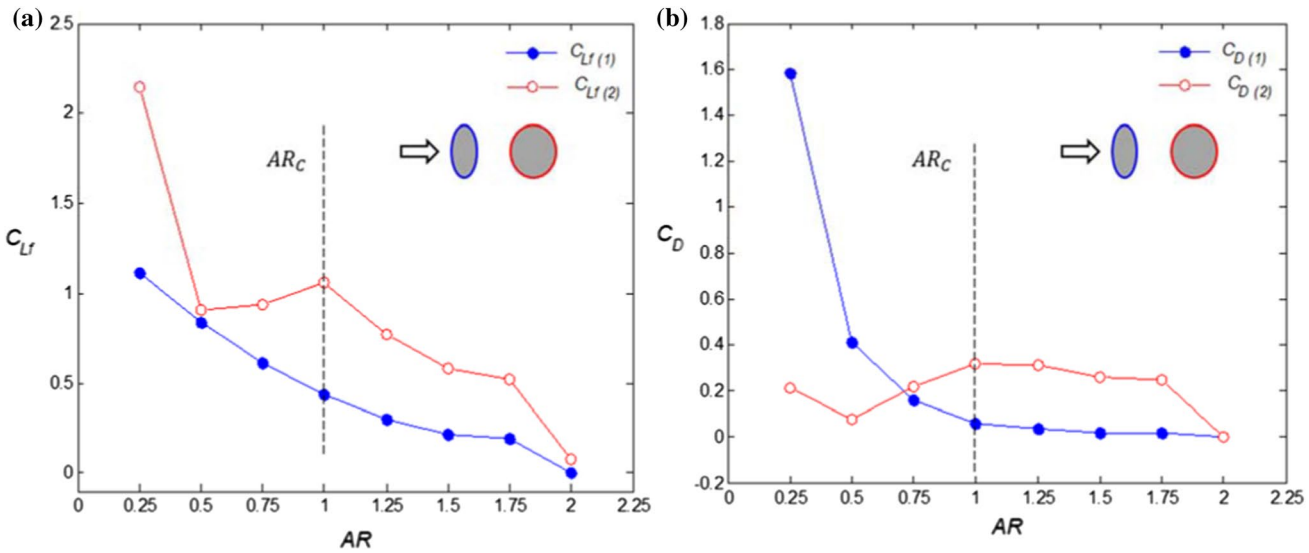

Fig. 12 Variation of the fluctuating of lift (rms) and time-averaged drag coefficient as a function of the aspect ratio for the upstream and downstream cylinders at Re = 200

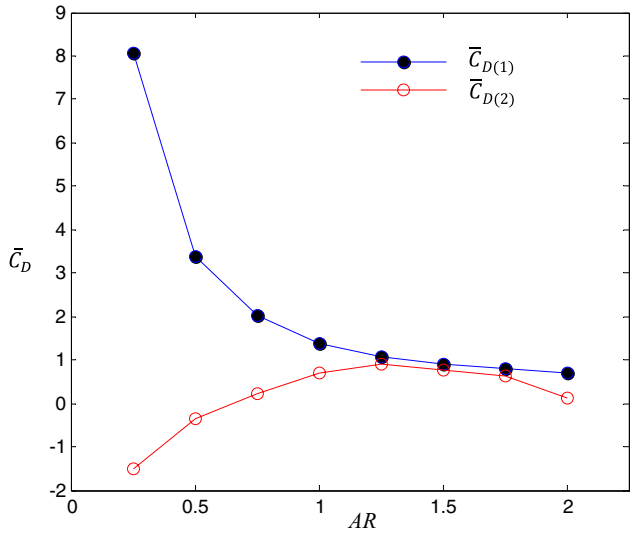

Fig. 13 Variation of the mean-drag coefficient as a function of the aspect ratio for the upstream and downstream cylinders at Re = 200

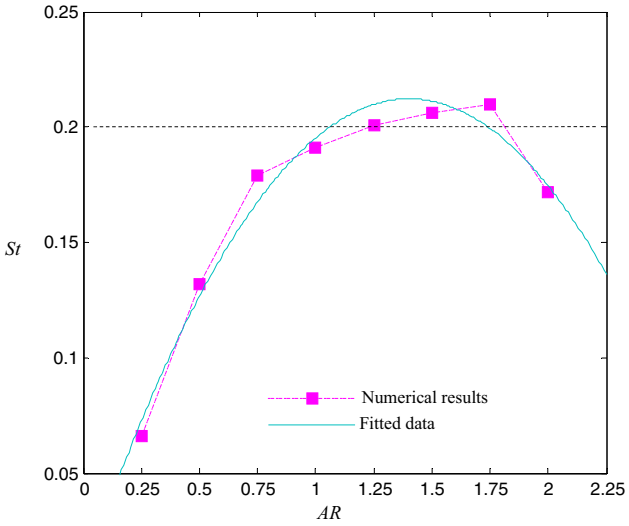

Fig. 14 Variation of the Strouhal number as a function of aspect ratio, including a fitted curve for the obtained numerical results

The results of the time-averaged drag coefficients of the cylinders are shown in Fig. 13. In general, the results reveal that the upstream elliptical cylinder undergoes a larger $\overline{C}_{\mathrm{D}}$ as compared with the downstream cylinder. It is found that the time-averaged drag coefficients of the upstream cylinder show a significant drop when *AR* increases. Besides, the amplitude of the fluctuating drag coefficient is larger for the upstream cylinder as compared with that of the downstream cylinder. For the downstream cylinder, it is seen that the time-averaged drag is negative at *AR* = 0.25 and 0.5 meaning that the downstream cylinder is pushed forwards by the fluid. The drag, then, gently increases to positive values by further increasing *AR*. Indeed, $\overline{C}_{\mathrm{D}}$ of the downstream cylinder neither approaches that of the upstream cylinder nor a single circular cylinder, even for maximum G^*.

Interestingly, the presence of the downstream cylinder causes a significant reduction of $\overline{C}_{\mathrm{D}}$ of the upstream cylinder. The reason for this reduction is the increment of the pressure in the separated wake behind the upstream cylinder. This increment of the pressure occurs when the vortices of the upstream and downstream cylinders are in in-phase mode. This concept has been proved earlier for two and three tandem circular cylinders at Re = 200 [22, 64, 69–72].

3.4 Relationship between St and *AR*

The variation of St as a function of *AR* is shown in Fig. 14. It is seen that *St* significantly increases by growing *AR* as expected. The variation of *St* starts from St = 0.065 at *AR* = 0.25 and continues to the maximum value of St = 0.211 at *AR* = 1.75. This trend can be formulated by showing the relationship between St and *AR* to facilitate the estimation of St at other *AR*, which is arranged between the test cases studied in this paper. Therefore, a curve is fitted on the trend of Strouhal number versus the aspect ratio. As a result, an equation is driven and identified as shown in Fig. 14. The equation can be written as follow:

$$\mathrm{St} = -0.11AR^2 + 0.3AR + 0.0053 \tag{7}$$

Evaluating the residuals is very valuable to understand the accuracy of the fitted curve on the trend of St versus the *AR*. It is found that the residuals approximate positive and negative errors randomly with less than 1.5% differentiation. Thus, Eq. (7) fits the data very well and can be applied with a 1.8% error.

4 Conclusions

In the present paper, a 2D laminar flow over elliptical tandem cylinders was studied numerically. The previously published studies of flow over an elliptic cylinder mostly estimated the hydraulic diameter of the elliptic cylinder by a diameter of a circular cylinder. In the case of using the hydraulic diameter, in some studies, the details of the calculation are missing, and the details have not been provided. In this study, there was an attempt to evaluate the correct hydraulic diameter due to its importance on all the fluidic parameters, using the Ramanujan theorem.

The percentage of the errors was highlighted considering the precise hydraulic diameter of the elliptical cylinder. Once using NEC the maximum error of evaluating Re

approximately reaches 180%. It was also found that this error reaches 25% for PEC.

The results show that the peak of pressure fluctuation of the upstream cylinder ($C_{Pf(1)}$) occurs at about 90° for $AR = 0.25$. The sinusoidal trend, then, is generated after a peak. The peaks of pressure fluctuation of the downstream cylinders with $AR = 0.25$ and 0.5 occur at 68° and 60°, respectively. These peaks are larger than those with higher aspect ratios except $AR = 2.0$. It was found that further increasing AR to 0.75, the peak of $C_{Pf(2)}$ approximately 30% rises as compared to pressure fluctuation of $AR = 0.5$. The pressure fluctuations become very low around both cylinders for the test case with $AR = 2.0$. Thus, the imposed forces on both cylinders with $AR = 2.0$ become minimum.

Based on the imposed pressure on the cylinders, it was observed that by altering the aspect ratio, the phase lag between the sinusoidal lift coefficients of the cylinders varies and it steadily reduces. The phase lag reaches the minimum at $AR = 1.5$ and it slightly increases again by the increment of AR to 2.0.

The results reveal that the upstream elliptical cylinder undergoes a larger $\overline{C}_D$ as compared with the downstream cylinder. The time-averaged drag coefficients of the upstream cylinder significantly drop by increasing AR. Besides, the amplitude of the fluctuating drag coefficient is larger for the upstream cylinder as compared with that of the downstream cylinder. For the downstream cylinder, it is seen that the time-averaged drag is negative at $AR = 0.25$ and 0.5. This means that the downstream cylinder is pushed forwards by the fluid. By further increasing AR, the drag slightly increases to positive values.

Based on the generated phase lag between forces and accordingly vortices, the Strouhal number varies. The minimum $St = 0.065$ occur at $AR = 0.25$, and it is regularly increased to the maximum value of $St = 0.211$ at $AR = 1.75$. The St of tandem elliptic cylinders becomes close to the vortex frequency formation of a single cylinder when $1.25 \leq AR \leq 1.75$ (e.g., $St \approx 0.2$). When AR increases to 2.0, vortex shedding frequency with 15% drops reaches $St = 0.17$ due to the minimum gap ratio between the cylinders. As a result, the relationship between the Strouhal number and AR was deduced and identified with high accuracy and a reasonable error of 1.8%.

Declarations

Conflict of interest The authors declare that they have no conflict of interest.

References

1. Igarashi T (1981) Characteristics of the flow around two circular cylinders arranged in tandem (first report). Bull JSME 24:323–331
2. Huhe-Aode TM, Taneda S (1985) Visual studies of wake structure behind two cylinders in tandem arrangement. Rep Res Inst Appl Mech (Kyushu Univ Jpn) 32(99):1–20
3. Zdravkovich MM (1987) The effects of interference between circular cylinders in cross flow. J Fluids Struct 1:239–261
4. Ljungkrona L, Norberg C, Sunden B (1991) Free-stream turbulence and tube spacing effects on surface pressure fluctuations for two tubes in an in-line arrangement. J Fluids Struct 5:701–727
5. Ljungkrona L, Sunden B (1993) Flow visualization and surface pressure measurement on two tubes in an inline arrangement. Exp Therm Fluid Sci 6:15–27
6. Derakhshandeh JF, Arjomandi M, Cazzolato B, Dally B (2012) Numerical simulation of vortex-induced vibration of elastic cylinder. In: Proceedings of international conference "18th Australasian fluid mechanics conference.
7. Xu G, Zhou Y (2004) Strouhal numbers in the wake of two inline cylinders. Exp Fluids 37:248–256
8. Sakamoto H, Haniu H, Obata Y (1987) Fluctuating forces acting on two square prisms in a tandem arrangement. J Wind Eng Ind Aerodyn 26:85–103
9. Hourigan K, Thompson MC, Tan BT (2001) Self-sustained oscillations in flows around long blunt plates. J Fluids Struct 15:387–398
10. Alam MM, Moriya M, Takai K, Sakamoto H (2002) Suppression of fluid forces acting on two square cylinders in a tandem arrangement by passive control of flow. J Fluids Struct 16:1073–1092
11. Johnson S, Thompson M, Hourigan K (2004) Predicted low frequency structures in the wake of elliptical cylinders. Eur J Mech-B/Fluids 23(1):229–239
12. Tan BT, Thompson MC, Hourigan K (2004) Flow past rectangular cylinders: respectively to transverse forcing. J Fluid Mech 515:33–62
13. Sohankar A (2011) A numerical investigation of the flow over a pair of identical square cylinders in a tandem arrangement. Int J Numer Methods Fluids 70:1244–1257
14. Derakhshandeh JF, Alam M (2019) A review of bluff body wakes. J Ocean Eng 182:475–488
15. Derakhshandeh JF, Alam MM (2019) A numerical study of heat transfer enhancement by a rectangular cylinder placed parallel to the heated wall. J Heat Transf. https://doi.org/10.1115/1.4043212
16. Alam MM, Moriya M, Takai K, Sakamoto H (2003) Fluctuating fluid forces acting on two circular cylinders in a tandem arrangement at a subcritical Reynolds number. J Wind Eng Ind Aerodyn 91:139–154
17. Alam MM, Zhou Y (2007) Phase lag between vortex shedding from two tandem bluff bodies. J Fluids Struct 23:339–347
18. Zhou Y, Yiu MW (2006) Flow structure, momentum and heat transport in a two-tandem-cylinder wake. J Fluid Mech 548:17–48
19. Kim S, Alam MM, Sakamoto H, Zhou Y (2009) Flow-induced vibrations of two circular cylinders in tandem arrangement, part 1: characteristics of vibration. J Wind Eng Ind Aerodyn 97:304–311
20. Alam MM, Meyer JP (2013) Global aerodynamic instability of twin cylinders in cross flow. J Fluids Struct 41:135–145
21. Alam MM (2014) The aerodynamics of a cylinder submerged in the wake of another. J Fluids Struct 51:393–400
22. Alam MM (2016) Lift forces induced by the phase lag between the vortex sheddings from two tandem bluff bodies. J Fluids Struct 65:217–237
23. Derakhshandeh JF, Gharib N (2020) Laminar flow instabilities of a grooved circular cylinder. J Braz Soc Mech Sci Eng 42(11):1–16

24. Roshko A (1960) Experiments on the flow past a circular cylinder at very high Reynolds number. Calif Inst Technol 10:345–356
25. Williamson CHK (1996) Three dimensional vortex dynamics in bluff body wake. J Exp Therm Fluid Sci 12:150–168
26. Chyu C, Rockwell D (1996) Evolution of patterns of streamwise vorticity in the turbulent near wake of a circular cylinder. J Fluid Mech 320:117–137
27. Norberg C (2003) Fluctuating lift on a circular cylinder: review and new measurements. J Fluids Struct 17:57–96
28. Brika D, Laneville A (1999) The flow interaction between a stationary cylinder and a downstream flexible cylinder. J Fluids Struct 13:579–606
29. Kravchenko AG, Moin P (2000) Numerical studies of flow over a circular cylinder at Re = 3900. Phys Fluids 12(2):403–417
30. Gu F, Wang JS, Qiao XQ, Huang Z (2012) Pressure distribution, fluctuating forces and vortex shedding behaviour of circular cylinder with rotatable splitter plates. J Fluids Struct 28:263–278
31. Derakhshandeh JF, Alam MM (2020) Reynolds number effect on the flow past two tandem cylinders. Wind Struct 30(5):475–483
32. Igarashi T (1986) Local heat transfer from a square prism to an airstream. Int J Heat Mass Flow 29:777–784
33. Sohankar A, Norberg C, Davidson L (1999) Simulation of three-dimensional flow around a square cylinder at moderate Reynolds numbers. Phys Fluids. https://doi.org/10.1063/1.869879
34. Sohankar A, Norberg C, Davidson A (1999) Large Eddy simulation of flow past a square cylinder: comparison of different subgrid scale models. J Fluids Eng 122:39–47
35. Saha AK, Muralidhar K, Biswas G (2003) Three-dimensional study of flow past a square cylinder at low Reynolds numbers. Int J Heat Fluid Flow 24:54–66
36. Sohankar A (2006) Flow over a bluff body from moderate to high Reynolds numbers using large eddy simulation. Comput Fluid 35(10):1154–1168
37. Mahir N (2009) Three-dimensional flow around a square cylinder near a wall. J Ocean Eng 36:357–367
38. Bai HL, Alam MM (2018) Dependence of square cylinder wake on Reynolds Number. J Phys Fluids 30(1–19):015102
39. Sheridan J, Hourigan K, Mills R (1997) Vortex structures in flow over a rectangular plate. J Fluid Struct Interact Aero-elast Flow-Induced Vib Noise 53:85–91
40. Mills R, Sheridan J, Hourigan K (2003) Particle image velocimetry and visualization of natural and forced flow around rectangular cylinders. J Fluid Mech 478:299–323
41. Johnson S, Thompson M, Hourigan K (2001) Flow past elliptical cylinders at low Reynolds numbers. In: Proceedings of 14th Australian fluid mechanics conference, Adelaide, pp 1–5
42. Faruquee Z, Ting D, Fartaj A, Barron R, Carriveau R (2007) The effects of axis ratio on laminar fluid flow around an elliptical cylinder. Int J Heat Fluid Flow 28(5):1178–1189
43. Bharti RP, Sivakumar P, Chhabra RP (2008) Forced convection heat transfer from an elliptical cylinder to power-law fluids. Int J Heat Mass Transf 51:1838–1853
44. Sen S, Mittal S, Biswas G (2012) Steady separated flow past elliptic cylinders using a stabilized finite-element method. CMES 2046(1):1–27
45. Paul I, Arul Prakash K, Vengadesan S (2014) Numerical analysis of laminar fluid flow characteristics past an elliptic cylinder: a parametric study. Int J Numer Methods Heat Fluid Flow 24(7):1570–1594
46. Raman SK, Prakash KA, Vengadesan S (2014) Effect of axis ratio on fluid flow around an elliptic cylinder—a numerical study. J Fluids Eng 135:111201–1
47. Alawadhi EM (2015) Numerical simulation of flow past an elliptical cylinder undergoing rotationally oscillating motion. J Fluids Eng 137(3):031106
48. Knauss DT, John JEA, Marks CH (1976) The vortex frequencies of bluff cylinders at low Reynolds numbers. J Hydronautics 10:121–126
49. Ota T, Nishiyama H, Taoka Y (1984) Heat transfer and flow around an elliptic cylinder. J Heat Mass Transf 27:1771–1779
50. Liu CH, Chen J (2002) Observations of hysteresis in flow around two square cylinders in a tandem arrangement. J Wind Eng Ind Aerodyn 90(9):1019–1050
51. Sohankar A, Etminan A (2008) Forced-convection heat transfer from tandem square cylinders in cross flow at low Reynolds numbers. Int J Numer Methods Fluids. https://doi.org/10.1002/fld.1909
52. Chatterjee D, Amiroudine S (2010) Two-dimensional mixed convection heat transfer from confined tandem square cylinders in cross-flow at low Reynolds numbers. Int Commun Heat Mass Transf 37:7–16
53. Takeuchi T, Matsumoto M (1992) Aerodynamic response characteristics of rectangular cylinders in tandem arrangement. J Wind Eng Ind Aerodyn 41(1–3):565–575
54. Valencia A (1996) Unsteady flow and heat transfer in a channel with a built-in tandem of rectangular cylinders. Numer Heat Transf Part A Appl Int J Comput Methodol 29(6):613–623
55. Zhao M, Cheng L, An H, Lu L (2014) Three-dimensional numerical simulation of vortex-induced vibration of an elastically mounted rigid circular cylinder in steady current. J Fluids Struct 50:292–311
56. Leontini JS, Griffith MD, Jacono DL, Sheridan J (2018) The flow-induced vibration of an elliptical cross-section at varying angles of attack. J Fluids Struct 78:356–373
57. Vijay K, Srinil N, Zhu H, Bao Y, Zhou D, Han Z (2020) Flow-induced transverse vibration of an elliptical cylinder with different aspect ratios. Ocean Eng 214:107831
58. Nair KM, Prasad SV, Nair VS (2020) Comparison of flow features near the wake of circular and elliptical cylinders for different gap to diameter ratios. In: Recent Asian research on thermal and fluid sciences. Springer, Singapore, pp 409–419
59. Chandrupatla TR, Osler TJ (2010) The perimeter of an ellipse. Math Sci 35:122–131
60. Villarino MB (2008) Ramanujan's Perimeter of an Ellipse. Escuela de Matematica, Universidad de Costa Rica. http://arxiv.org/abs/math/0506384v1. Accessed 10 2013
61. Sarkar S, Sarkar S (2010) Vortex dynamics of a cylinder wake in proximity to a wall. J Fluids Struct 26(1):19–40
62. Derakhshandeh JF, Arjomandi M, Dally B, Cazzolato B (2014) The effect of arrangements of two circular cylinders on the maximum efficiency of vortex-induced vibration power using a scale-adaptive simulation model. J Fluids Struct 49:654–666
63. Zafar F, Alam MM (2018) A low Reynolds number flow and heat transfer topology of a cylinder in a wake. Phys Fluids 30(8):083603
64. Alam MdM, Zheng Q, Derakhshandeh JF, Rehman S, Ji C, Zafar F (2018) On forces and phase lags between vortex sheddings from three tandem cylinders. Int J Heat Fluid Flow 69:117–135
65. Koda Y, Lien FS (2013) Aerodynamic effects of the early three-dimensional instabilities in the flow over one and two circular cylinders in tandem predicted by lattice Boltzmann method. Comput Fluids 74:32–43
66. Dehkordi BG, Moghaddam HS, Jafari HH (2011) Numerical simulation of flow over two circular cylinders in tandem arrangement. J Hydrodyn 23(1):114–126
67. Park J, Kwon K, Choi H (1998) Numerical solutions of flow past a circular cylinder at Reynolds numbers up to 160. KSME Int J 12(6):1200–1205

68. Sharman B, Lien FS, Davidson L, Norberg C (2005) Numerical predictions of low Reynolds number flows over two tandem circular cylinders. Int J Numer Methods Fluids 47(5):423–447
69. Derakhshandeh JF (2015) Harnessing hydrokinetic energy from vortex-induced vibration (VIV). Doctoral dissertation
70. Derakhshandeh JF, Arjomandi M, Dally B, Cazzolato B (2015) Harnessing hydro-kinetic energy from wake induced vibration using virtual mass spring damper system. J Ocean Eng 108:115–128
71. Derakhshandeh JF, Arjomandi M, Dally B, Cazzolato B (2016) Flow-induced vibration of an elastically mounted airfoil under the influence of oncoming vortices. J Exp Therm Fluid Sci 74:58–72
72. Alam M, Derakhshandeh JF, Zheng Q, Rehman S, Ji C, Zafar F (2017) The flow around three tandem cylinders. Advances in structural engineering and mechanics, Korea